ACS Catalysis

pubs.acs.org/acscatalysis Research Article

Controlling Selectivity and Stability in the Hydrocarbon Wet-Reforming Reaction Using Well-Defined Ni + Ga Intermetallic Compound Catalysts

Yuanjun Song, Yang He, and Siris Laursen*

Cite This: *ACS Catal.* 2020, 10, 8968–8980 Read Online

ACCESS | Metrics & More | Article Recommendations | Supporting Information

ABSTRACT: In this study, we present the use of compositionally and structurally well-defined, oxide-supported nanoparticle Ni + Ga intermetallic compound (IMC) catalysts in the wet reforming of propane. The definition of the IMC catalysts allowed for more direct connections to be made between catalyst bulk and surface compositions and catalyst performance in wet reforming. We show that Ni + Ga catalysts exhibit comparable or better rates of reaction on a per-site basis and improved stability in comparison to other leading formulations. We also demonstrate excellent control over product selectivity as a function of Ni + Ga IMC bulk and surface compositions with nearly ideal selectivity toward CO_2/H_2 or CO/H_2 achieved. Selectivity toward the production of smaller hydrocarbons could also be suppressed significantly due to uniquely limited rehydrogenation kinetics of the Ni + Ga IMCs. Our studies also shed light on the stability of Ni + Ga IMCs under reaction conditions and how high conversion in reactions that involve many strongly bound reaction intermediates can lead to IMC phase relaxation to the most stable phase with concomitant surface composition and catalytic performance changes. Correlations between surface chemistry and catalyst performance were afforded by both the well-defined nature of the IMCs and computational surface science studies.

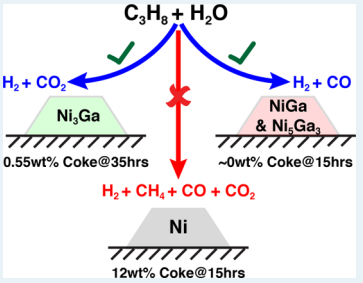

KEYWORDS: *model catalyst materials, non-noble metal catalysts, surface science, rational catalyst design, propane wet reforming*

I. INTRODUCTION

Catalytic wet reforming of hydrocarbons (HCs) and newer oxygenated feedstocks continues to be a vital process for the production of H_2 (H_2/CO_2) and synthesis gas (H_2/CO) for the chemical industry.[1−7] Despite its central role in H_2 and synthesis gas (H_2/CO) productions, the community still lacks a clear and complete mechanistic understanding that would enable the development of new and improved catalysts. This is partially due to mechanistic complexity apart from kinetically controlling reaction steps and the need for elevated surface reactivity to drive C−H and C−C activations. These issues persist as the community moves to develop catalysts for the dry reforming of CH_4 and the reforming of small bio-derived oxygenates. Balancing stability, selectivity, and overall activity is also still a challenge since the three phenomena are often found to be kinetically connected, dependent upon the reaction environment, and crucial to optimize the economic viability of the process. Stable and appropriately active catalysts that achieve ideal H_2/CO_2 or H_2/CO product distributions with little unselective CO or CH_4 produced are also still lacking. Herein, we present a study focused on using compositionally and structurally well-defined intermetallic compound (IMC) catalysts composed of Ni and Ga (Ni_3Ga, Ni_5Ga_3, and NiGa) to better understand the fundamental aspects of the wet-reforming reaction mechanism and connect catalyst performance to surface chemical features.

The catalytic reforming reaction mechanism inherently presents unique challenges for catalyst design due to catalyst surface reactivity affecting the rate-determining steps early in reactant activation pathways, as well as surface reaction steps late in the kinetic network that dictate product selectivity and the formation of coke or TM carbide. The recalcitrance of saturated hydrocarbon (HC) reactants often necessitates the use of catalytic metals with high reactivity toward carbon to drive the C−H bond activation. However, this approach often promotes coke or TM carbide formation if C/CH_x species are not effectively kinetically coupled with the oxidizer supply or oxidation events for CO or CO_2 production. In dictating CO vs CO_2 selectivity, both the surface chemistry toward C and O plays a role, which connects efforts to improve C−H activation and catalyst stability with the overall product selectivity. Likewise, the control of unselective rehydrogenation kinetics and the loss of H to lighter HCs must also be suppressed and are dependent upon the surface chemistry toward C and H. These complexities are compounded by the oft observed shift

Received: March 17, 2020
Revised: June 12, 2020
Published: July 17, 2020

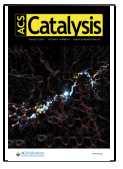

https://dx.doi.org/10.1021/acscatal.0c01261
ACS Catal. 2020, 10, 8968–8980

in the available surface reaction sites as a function of time-on-stream (TOS), inhomogeneous distribution of sites responsible for each aspect of the reaction mechanism, and purposefully selected reaction conditions such as the steam-to-carbon ratio. In the end, there is a great amount of molecular-level understanding that still needs to be developed with respect to what constitutes a balanced surface chemistry toward C, O, and H and the superstructure effects of a thoroughly connected kinetic network. A review of specific efforts in each of these regards follows.

Many prior studies have focused on limiting coke, TM carbide, and carbon nanotube (CNT) formation through the addition of secondary elements to a late TM metal like Ni to attenuate C/CH_x supply at the catalyst surface.[2,5,6,8−15] For example, the addition of mostly inactive coinage metals (Au or Ag) or large p-block elements (Bi) has been shown to block over-reactive sites via a simple physical effect.[8−10,13,14] Stability could also be improved by reducing the rate of C−H activation in comparison to that of the over-reactive sites of pure Ni through the addition of more reactive TMs and f-block elements. For example, the addition of Fe, Mo, Co, or Rh results in the lower overall catalytic activity in comparison to that of Ni at t = 0 TOS but improved stability. Because the added elements limit coke deposition, their overall activity at steady state is often higher than that of pure Ni.[4,15−17] When doping late TMs with large p-elements (Sn, Pb, Te, etc.) that form oxides too stable to cycle in composition under reaction conditions, the over-reactive site blocking or electronic modifications of the general surface chemistry likely limit C−H activation and coke deposition.[3,6,8,18−21]

Other efforts have aimed to modify the dynamics of the oxidation portion of the kinetic network. Specifically, dopants may affect oxidizer activation, oxidation step kinetics, or oxidizer intermediate surface coverages. Oxygen storage effects may also be employed to simply preserve sites responsible for oxidizer supply in the face of unavoidable coke deposition. This effect has been observed in catalyst formulations that employ lanthanide elements as dopants (Ce, La, and Yb), as well as with other TMs (Mo and Fe) that form reducible oxides under reaction conditions.[4,15,16,22,23] Surface reactivity toward oxygen and oxidizer fragments may also be modified through the addition of p-block elements and the formation of parent metal particles with a shell of ill-defined IMC.[3,6,18,24] Because H_2O dissociation and oxidation step kinetics are often not kinetically limiting, the effect of these dopants on individual reaction mechanism steps is less well quantified.

Controlling CO vs CO_2 selectivity is equally important in the design of high-performance reforming catalysts and is dependent upon the oxidizer supply rate, as well as oxidation step kinetics. Many studies have already illustrated the effect of adding more oxophilic early TMs, early f-block elements, and p-block elements in modifying the CO vs CO_2 selectivity.[3−5,15,16,22,23] The addition of lanthanide elements (La, Ce, and Yb) and early TMs (Mo and Fe) to Ni catalysts has been shown to shift the selectivity toward CO production.[4,15,16,22,23] The origin of the selectivity differences may be slower oxidation step kinetics that promote CO production over CO_2. This approach appears to also have a favorable effect in limiting the carbon chemical potential at the catalyst surface by increasing O/OH surface coverages. On the other hand, CO_2 can be promoted by weakening CO and O/OH adsorptions on the catalyst surface and is most readily visible over pure Ni and in low-temperature reforming of small oxygenates where aggressive reactivity to drive C−H activation is not needed.[3,5,6,25,26] The addition of Fe to Co/Al_2O_3 in the wet reforming of toluene showed a slight increase in CO_2 vs CO selectivity as well.[27]

In the end, all of these efforts highlight the need for a balanced C−H and oxidizer activation and balanced surface intermediate coverages to achieve the enhanced overall activity, as has already been proposed by others.[28−30] Specifically, the overly rapid C−H activation is limited and the C/CH_x oxidation is slowed to balance surface intermediate coverages or build in dual reaction sites that individually perform C−H activation and H_2O dissociation.

With respect to controlling the fate of atomic H in H_2 evolution vs unselective rehydrogenation of C/CH_x species, less clear trends are provided by prior studies. However, the addition of elements that form stronger bonds to and modify the electronic structure of the parent element appears to limit rehydrogenation. For example, the addition of both Mo to Ni and Ce to Rh suppresses hydrogen loss to CH_4.[4,17] Shifting the Fermi level of Ni via Na or K doping has also been shown to limit unselective rehydrogenation in acetic acid steam reforming.[31] Each of these approaches clearly limits rehydrogenation kinetics by modifying the stability of carbonaceous or atomic H intermediates or the fundamental nature of the hydrogen-surface bond. A similar trend has been identified in prior studies by others and ourselves in the surface chemistry of TM solid compounds formed from TMs combined with similarly sized p-block elements.[8,32,33] Elevated kinetic barriers for H-transfer have been connected to the nature of the H-surface bond and the presence of covalent-like bonding within the TM solid compound as a function of the selective or full hybridization between the d- and p-states of constituent elements.[20,21,33,34] This effect may help to avoid the unselective loss of H, but may also detrimentally affect H_2 evolution rates in reforming reactions. The studies presented herein clarify the beneficial effect of this newly accessible surface chemistry.

It is without a doubt that significant insights have been derived from the greater body of prior studies focused on wet reforming. However, even more precise structure−activity relationships must be developed due to the complexity of the catalytic reaction system. Unfortunately, most prior studies utilized catalytic materials that were less well defined at the atomic scale. Of specific issue is the definition of the catalyst particle surface composition and reaction site distribution as a function of the identity of constituent elements and their respective amounts in the catalyst formulation. Because the bonding between late TMs and dopant elements varies considerably as a function of both elements, many material structures can be produced from well-distributed dopants to core−shell structures to nonwetting islands of the secondary element.[3,5,6,15,24,35−37] These structural and compositional complexities limit the resolution of the structure−activity relationships developed when studying these materials. Our studies have focused upon producing and investigating well-defined materials such that the features that obscure connections between performance and surface chemistry can be avoided.

As an overview, we demonstrate the synthesis and use of compositionally and structurally well-defined IMC catalysts composed of Ni and Ga in the wet reforming of propane and connect their surface chemistry to favorable changes in their catalytic chemistry. We outline the synthesis of well-defined

https://dx.doi.org/10.1021/acscatal.0c01261
ACS Catal. 2020, 10, 8968−8980

oxide-supported Ni + Ga IMC nanoparticles (Ni_3Ga, Ni_5Ga_3, and NiGa) that exhibit phase-pure bulk crystal structure and bulk-like or off-stoichiometric surface composition. By investigating three Ni + Ga IMC compositions (Ni_3Ga, Ni_5Ga_3, and NiGa), we were also able to shed light upon the effect of systematic changes in surface chemistry on catalytic performance, as well as the stability of the materials under preparation and reaction conditions. Computational surface science approaches in the density-functional theory (DFT) framework were applied to the well-defined materials to connect the observed catalyst performance with their surface chemistry in critical reaction steps within the reforming mechanism. Results show excellent control over coke formation, unselective light HC production, and H_2/CO vs H_2/CO_2 selectivity and clear connections with changes in the Ni + Ga IMC surface chemistry as a function of bulk and surface compositions.

II. METHODS

A. Catalyst Synthesis and Characterization. Significant advancements in the synthesis of well-defined IMCs with pure bulk phase and bulk-like terminated surfaces have been achieved in our group. This development was critical to enable enhanced connections between IMC catalyst formulation and their catalytic surface chemistry.[20,21] The major phenomena found to control IMC synthesis as oxide-supported nanoparticles were (1) the availability and diffusion of reduced metal elements on the oxide support, (2) a strong effect of H_2 chemical potential during particle formation, (3) stabilizing and growing the particles via annealing, and (4) the surface chemistry of support toward the constituent elements of the IMC. A fundamental understanding of these effects, which will be published in a follow-up report, allowed for the production of 10 wt % SiO_2-supported Ni + Ga (Ni_3Ga, Ni_5Ga_3, and NiGa) IMCs with nearly pure bulk crystal phases and bulk-like particle surface termination (NiGa and Ni_3Ga) or core−shell structures (Ni_5Ga_3).

In short, SiO_2-supported Ni + Ga catalysts (Ni_3Ga, Ni_5Ga_3, and NiGa) were synthesized by depositing a defined amount of $Ni(NO_3)_2$*$6H_2O$ (Sigma-Aldrich) and $Ga(NO_3)_3$*H_2O (Sigma-Aldrich) metal precursors on SiO_2 (Alfa Aesar, amorphous fumed, 350−420 m^2/g) via the incipient wetness impregnation method. The total metal weight loading is 10 wt % for all IMC catalysts. Inductively coupled plasma atomic emission spectroscopy (ICP-AES) was used to verify the agreement between the target and actual loadings. Both $Ni(NO_3)_2$ and $Ga(NO_3)_3$ were dissolved in a small amount of 30 wt % nitric acid solution at 70 °C. The metal salt solution was then deposited on the SiO_2 support and stirred until the paste was homogeneous and dry enough to transfer to a pretreatment tube. After the deposition, the catalysts were dried under an Ar flow for 12 h at 100 °C. As-reduced Ni_3Ga/SiO_2, Ni_5Ga_3/SiO_2, and $NiGa/SiO_2$ were produced by reduction under a 100% H_2 flow at 700 °C for 2 h. The annealed Ni_3Ga/SiO_2, Ni_5Ga_3/SiO_2, and $NiGa/SiO_2$ were produced by annealing the as-reduced catalysts under 100% Ar at 700 °C for 12 h. For reduced Ni/SiO_2, 10 wt % Ni was loaded on the SiO_2 support via the incipient wetness impregnation method and then reduced under 100% H_2 at 500 °C for 2 h. In performance tests, all catalysts were pretreated *in situ* and switched to reaction conditions without contacting air. Before characterization, each catalyst was passivated in 1% O_2/Ar at room temperature for 1 hr to prevent the autocatalytic oxidation of the catalyst by ambient O_2 and then reduced *in situ*, if possible, before characterization.

Catalysts were characterized to determine their structural properties before and after reaction conditions (see Figure 1).

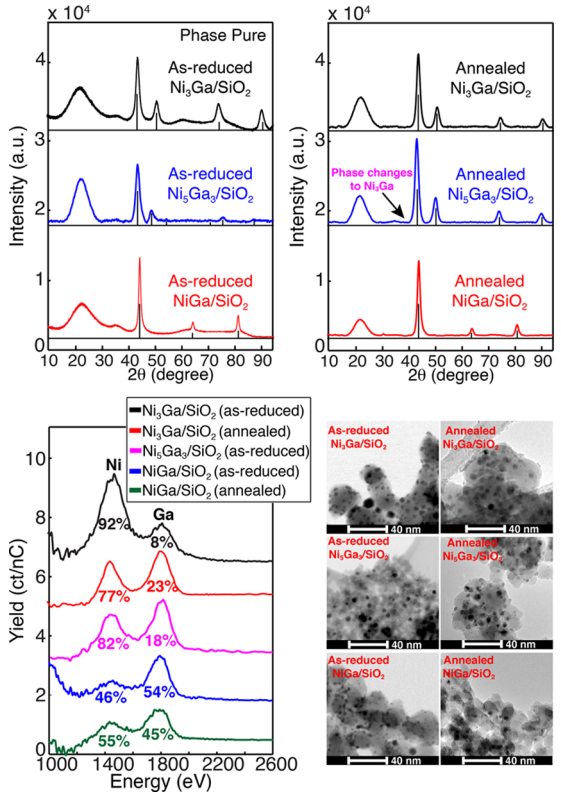

Figure 1. Long-acquisition-time powder X-ray diffraction (pXRD), high sensitivity-low energy ion scattering (HS-LEIS), and transmission electron microscope (TEM) characterizations for as-reduced and annealed SiO_2-supported Ni + Ga IMCs (Ni_3Ga, Ni_5Ga_3, and NiGa). HS-LEIS measurement was not performed for the annealed Ni_5Ga_3/SiO_2.

X-ray diffraction (XRD) and high resolution XRD (HR-XRD) were utilized to characterize the bulk crystal structure of the catalysts. Powder XRD with long acquisition times (4 h) and HR-XRD using synchrotron radiation showed that the bulk compositions of as-reduced SiO_2-supported Ni + Ga IMCs (Ni_3Ga/SiO_2, Ni_5Ga_3/SiO_2, and $NiGa/SiO_2$) were all nearly phase pure. After the annealing pretreatment, bulk phases of Ni_3Ga/SiO_2 and $NiGa/SiO_2$ were retained. However, the higher-energy bulk phase of Ni_5Ga_3/SiO_2 relaxed to Ni_3Ga because of lower phase stability.

High-sensitivity low-energy ion scattering (HS-LEIS), a more surface-sensitive technique, was used for the measurement of surface composition. Depth profiling of the annealed Ni_3Ga/SiO_2 was used for the HS-LEIS calibration to obtain response factors for Ni and Ga elements. The HS-LEIS data indicated that the surface composition of the as-reduced Ni_3Ga/SiO_2 was off-stoichiometric with a termination of 92% Ni and 8% Ga. However, the surface composition could be adjusted back to bulk-like by the annealing pretreatment (77% Ni and 23% Ga) with the sustained Ni_3Ga bulk phase purity. A similar phenomenon of Ni segregation to the surface after reduction pretreatment was also found in the case of as-reduced Ni_5Ga_3/SiO_2 (82% Ni and 18% Ga). However, annealing the as-reduced Ni_5Ga_3 led to a bulk phase change to

https://dx.doi.org/10.1021/acscatal.0c01261
ACS Catal. 2020, 10, 8968−8980

Ni_3Ga; thus, the material was deemed no longer well defined and not appropriate for further characterization by HS-LEIS. The surface compositions of the as-reduced and annealed $NiGa/SiO_2$ were found to be close to bulk-like terminated (46% Ni and 54% Ga for the as-reduced NiGa and 55% Ni and 45% Ga for the annealed NiGa). It is noted that the annealing treatment caused fairly minor particle size increases in Ni + Ga IMCs in all cases, e.g., from 2−5 to 4−8 nm. This is an interesting phenomenon since similar treatments applied to noble or alloy catalysts would lead to significant particle size increases.[38−41] The details of characterization and catalytic performance tests are outlined in the Supporting Information document.

B. Catalytic Activity Test. *1. Propane Steam Reforming Reaction.* All catalytic activity experiments were performed at the atmospheric pressure in the gas phase in a 0.5 inch quartz tube heated by a tube furnace. The catalyst bed consisted of the catalyst mixed with an 80 mesh SiC and was supported and capped by fine quartz wool plugs. The temperature of the catalyst bed was measured with a K-type thermocouple, which was located directly above the catalyst bed inside of the quartz tube. The flow rates of the gas reactants were controlled via mass flow controllers. Water was introduced using a custom-built precision syringe pump (4 μL/min). The reactor effluent gas was characterized by an online gas chromatograph (SRI) equipped with a HayeSep-D column and flame ionization (FID) and thermal conductivity detectors (TCDs). *In situ* pretreatment of the catalyst was performed directly before switching to reaction conditions. The feed composition for all tests was $H_2O/C_3H_8/Ar$ = 8.1/0.9/91, which equates to a steam-to-carbon ratio of S/C = 3. In the study of S/C effect, flow rate of steam was kept the same and flow rate of propane was increased, so feed compositions were 8.1/1.35/90.55 and 8.1/2.7/89.2 for S/C=2 and 1. All critical tests were performed in triplicate. Conversion and selectivity were calculated as follows

$$\text{conversion of } C_3H_8 = \frac{\text{mole flow rate of propane converted}}{\text{mole flow rate of propane feed}}$$

$$\text{production rate} = \frac{\text{mole flow rate of product X}}{\text{catalyst weight}} \quad (\mu\text{mol}/(\text{s} \times \text{g}))$$

$$\text{selectivity of X} = \frac{\text{production rate of X}}{\text{total production rates of all products}}$$

$$\text{TOF(propane)} = \frac{\text{mole flow rate of propane} \times \text{conversion}}{\text{catalyst weight} \times \text{IMC wt\%} \times \text{H}_2\text{ uptake}} (\text{s}^{-1})$$

Ideal product selectivity is defined as the highest selectivity achievable in the production of either a mixture of H_2 and CO_2 or H_2 and CO. In the case of H_2/CO_2 production (C_3H_8 + $6H_2O$ = $3CO_2$ + $10H_2$), the ideal selectivity is 77% H_2 and 23% CO_2. In the case of H_2/CO production (C_3H_8 + $3H_2O$ = 3CO + $7H_2$), the ideal selectivity is 70% H_2 and 30% CO.

Thermodynamic equilibrium conversion and selectivity with S/C = 3 at 400 and 600 °C were calculated using ASPEN HYSYS V11 simulation software. The following reactions were considered in the simulation

(1) $C_3H_8 + 3H_2O = 3CO + 7H_2$
(2) $C_3H_8 + 6H_2O = 3CO_2 + 10H_2$
(3) $C_3H_8 + 2H_2 = 3CH_4$
(4) $CO + H_2O = CO_2 + H_2$
(5) $CO + 3H_2 = CH_4 + H_2O$
(6) $CO_2 + 4H_2 = CH_4 + 2H_2O$

At both 400 and 600 °C, the equilibrium conversion of propane was 100%. At 400 °C, the equilibrium product distributions were 39.7% H_2, 40.2% CH_4, 0.4% CO, and 19.7% CO_2. At 600 °C, the equilibrium product distributions were 70.2% H_2, 5.2% CH_4, 8.5% CO, and 16.1% CO_2. The equilibrium conversion and selectivity trends are similar to the results reported in the literature.[42,43] It is important to note that these values are predictive only if the catalyst promotes both the forward and reverse reaction rates similarly. A properly designed catalyst would promote forward reactions while limiting reverse and unselective pathways.

2. Water Gas Shift Reaction. To further investigate the limited hydrogenation kinetics of the IMC catalysts, we utilized the water gas shift reaction to ascertain whether H_2 produced in the reaction hydrogenated CO to CH_4. The feed composition in the WGS tests was designed to mimic the H_2 and CO concentrations produced under the propane wet-reforming condition. The feed composition of CO was determined from the theoretical amount of CO produced as an intermediate during the propane wet-reforming reaction at a steady state. The feed of H_2O was the same as that used in the wet reforming.

C. DFT Calculation. Computational surface science studies in the density-functional theory (DFT) slab model framework were employed to correlate the basic surface chemical features with the observed catalytic activity and selectivity of the Ni + Ga IMCs. To enable reasonable connections between calculations and experimental observations, we focused our modeling efforts on the Ni + Ga IMCs that could be produced in well-defined compositional states where both the bulk and surface compositions of the IMCs were quantified. The IMCs modeled were Ni-rich Ni_3Ga modeled as a monolayer of Ni on $Ni_3Ga(111)$, stoichiometrically terminated $Ni_3Ga(111)$, and stoichiometrically terminated NiGa(110). Calculations were also performed for Ni(211) and Ni(111) surfaces to serve as a reference. The general surface reactivity toward C−H activation, H_2O dissociation, O, and CO was investigated by calculating the energetics of propane first dehydrogenation, H_2O dissociation, and CH_3 hydrogenation to CH_4, CO molecular adsorption, and O_2 dissociative adsorption. The finer details of the calculation are described in the Supporting Information document.

III. RESULTS

Catalytic reforming reactions, where the dramatic reorganization of elements occurs as reactants that are transformed into products, present kinetic networks that are expansive. The active mechanistic pathways within the greater network are a function of the catalyst surface chemistry and reaction conditions but may also shift as a function of time-on-stream as surface poisons modify the available reaction site distribution. It is also common that kinetically controlling steps are mechanistically removed from surface reaction steps that dictate selectivity and surface poison production. Because

https://dx.doi.org/10.1021/acscatal.0c01261
ACS Catal. 2020, 10, 8968−8980

of these complexities, we aimed to use compositionally and structurally well-defined catalytic materials such that more clear connections with the catalyst function could be achieved. Through significant efforts, we developed synthesis methods that could produce well-defined Ni + Ga IMCs (see Methods). Three Ni + Ga IMC compositions were investigated: Ni_3Ga, NiGa, and Ni_5Ga_3. The as-reduced catalysts exhibited particle surface compositions that were Ni-rich (92% Ni), bulk-like (46% Ni), and Ni_3Ga-like (82% Ni). High-temperature annealing for 12 h could adjust the Ni_3Ga and NiGa surface compositions to bulk-like with compositions of 77% Ni and 55% Ni, respectively. Annealing of Ni_5Ga_3 induced a bulk phase relaxation to Ni_3Ga; thus, the surface composition was not measured. Therefore, the materials available for study were bulk-like terminated Ni_3Ga and NiGa, Ni-rich Ni_3Ga, Ni_3Ga-terminated Ni_5Ga_3, and a Ni_5Ga_3 that changed to Ni_3Ga bulk with an unquantified surface composition. We coin the off-stoichiometrically terminated IMCs core−shell. The suite of available materials allowed for the effect of general surface reactivity and the concentration of Ni and Ga at the crystal surface on the catalytic surface chemistry to be investigated.

III.A. Monometallic Ni vs Ni-Rich and Stoichiometrically Terminated Ni_3Ga. To provide a benchmark for comparison, a monometallic reduced Ni catalyst was investigated under the same wet-reforming conditions used in the study of the Ni + Ga IMCs. These results illustrate key features in the reaction that need to be addressed, e.g., product selectivity, shifts in reaction site distribution, and deactivation via coke deposition (see Figure 2). Conversion over the Ni

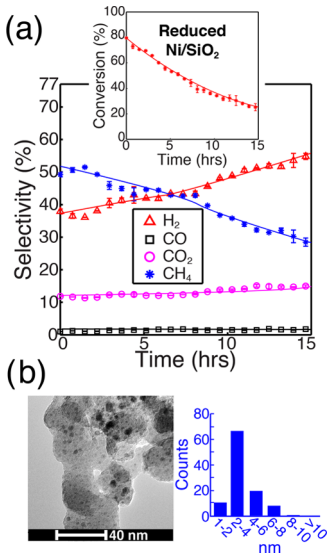

Figure 2. (a) Catalytic performance of the reduced Ni/SiO_2 in propane steam reforming at 400 °C with S/C = 3 and (b) TEM and size distribution measurement of the reduced Ni/SiO_2. The catalyst loading in the reaction was 100 mg for Ni/SiO_2.

catalyst was high (∼80%) at the start of the reaction, illustrating the known activity of Ni(211) and other high-energy sites in C−H activation.[12,44,45] Conversion quickly reduced over time as sites that perform rapid C−H activation were lost through site-specific coke or carbide formation (∼12 wt % coke/carbide after 15 h TOS shown in Figure S10). This phenomenon illustrated the rapid shift of active surface reaction sites when overly rapid C−H activation is not effectively coupled with oxidation. This lack of kinetic coupling is made more clear by the known rapid H_2O dissociation and $C/CH_x/CO$ oxidation steps over Ni, which have been illustrated in rate-order and D_2O kinetic isotope effect studies by others and here in the selectivity preference toward CO_2.[46,4746,47]

The origin of the changes in product selectivity as a function of the changing reaction site distribution over Ni catalysts has already been determined to a degree by others and may be used to scrutinize changes observed in the Ni + Ga IMC catalysts.[4,12,45,48] High-energy Ni sites are known for driving rapid C−H activation, but also limit oxidation kinetics due to the enhanced stability of reaction intermediates.[12,45,49−51] Nonetheless, oxidation kinetics even over high-energy Ni sites is still markedly rapid.[12,48] Therefore, as carbon selectively deposits and poisons high-energy Ni sites, the rate of C/CH_x supply slows, affecting unselective rehydrogenation and CH_4 production, yet does not affect CO vs CO_2 selectivity as markedly since oxidation is rapid over both high- and low-energy Ni reaction sites.[4] Regardless, the activity of Ni in the unselective rehydrogenation of C/CH_x fragments is still dominant in the catalyst performance and provides ample comparison with the Ni + Ga IMCs that show considerably limited CH_4 production. Our results and the established understanding of the surface chemistry of Ni illustrate the lack of control of the fate of atomic H in H_2 vs rehydrogenation and CH_4 production. It is also noted that Ni as a benchmark also indicates that rapid C−H activation is already within reach, but must be effectively coupled with oxidation events to avoid coke deposition.

To connect most clearly to the catalytic surface chemistry of monometallic Ni, we focus first on the as-reduced Ni_3Ga catalyst that exhibited a core−shell structure with a Ni-rich surface composition (92% Ni and 8% Ga) and Ni_3Ga core. The particle size average of the fresh catalyst was 3.5 nm and was only marginally increased after 16 h of TOS (see Figure 3c). The initial catalytic activity of the catalyst was reminiscent of monometallic Ni with similar propane conversion, unselective hydrogenation of C/CH_x fragments leading to CH_4, and reduced H_2 production (see Figure 3a). Despite this similarity, oxidation steps at the catalyst surface were clearly modified by the Ni_3Ga core or through the loss of Ni at the catalyst surface, changing the shell composition to more Ni_3Ga-like. CO selectivity was elevated to 8−9% at the start of the run in comparison to 1−2% over monometallic Ni. This suggested that the catalyst exhibited elevated surface reactivity toward either CO or O/OH that limited oxidation kinetics or limited O/OH supply by slower H_2O dissociation kinetics. Deactivation was similar to the monometallic Ni catalyst, with the initial conversion of ∼88% reduced via a second-order deactivation over the first 6 h. Deactivation then shifted to first-order from 6 to 20 h and then transitioned to the zeroth-order unlike the monometallic Ni catalyst (see Figure S1). The coke deposition was quantified using TGA as ∼1.3 wt % after 35 h of TOS significantly reduced in comparison to the Ni catalyst (∼12 wt %) (see Figure S10). In addition, bright-field TEM analysis post reaction showed no carbon nanotube formation, particle lift-off, or carbon-encapsulated IMC particles corroborating the TGA analysis. Likewise, long-acquisition-time (4 h) pXRD analysis of postreaction samples was unable to detect any carbide species. These results suggest that the rapid deactivation of Ni_3Ga/SiO_2 is mainly because of the loss of high-energy Ni surface sites via nickel carbonyl formation.

https://dx.doi.org/10.1021/acscatal.0c01261
ACS Catal. 2020, 10, 8968−8980

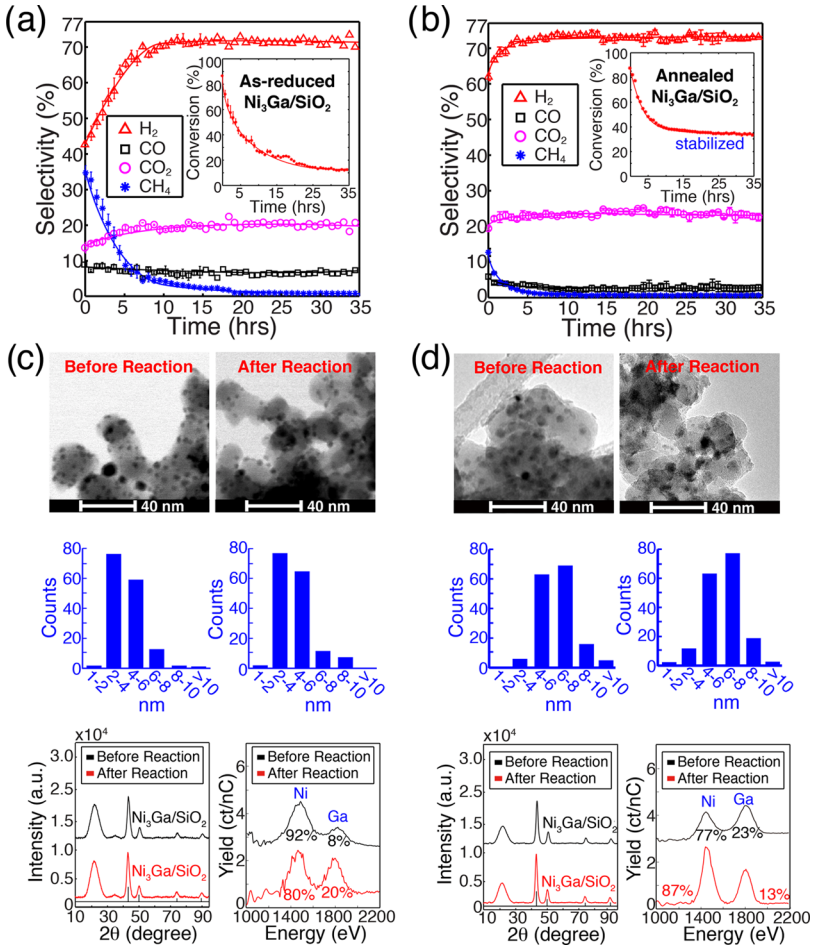

Figure 3. Catalytic performance of (a) the as-reduced Ni_3Ga/SiO_2 and (b) annealed Ni_3Ga/SiO_2 at 400 °C with S/C = 3, (c) and (d) TEM, particle size distribution, long-acquisition-time pXRD, and HS-LEIS characterization before and after reaction of the as-reduced Ni_3Ga/SiO_2 and annealed Ni_3Ga/SiO_2, respectively. Catalyst loading was 100 and 800 mg, respectively.

Interestingly, the temporal changes in individual product selectivity over the as-reduced Ni_3Ga were markedly different from those of pure Ni. The selectivity toward CH_4 rapidly diminished in the first ∼7 h to 5% and further reduced to nearly zero after ∼18 h under reaction conditions. HS-LEIS characterization post reaction indicated a loss of Ni (80% Ni and 20% Ga; see Figure 3c), likely via the Ni carbonyl formation, which resulted in deactivation as a function of TOS and diminished CH_4 production. This implicated the Ni-like surface chemistry in driving unselective rehydrogenation and bulk-like Ni_3Ga in limiting the unselective hydrogen loss. Interestingly, the shifts in reaction site distribution affect CO oxidation activity more than that over pure Ni, but the effect was still fairly marginal. Nonetheless, these results already suggest that unselective hydrogenation may be controlled and that oxidation rates can be modified.

Shifting to the structurally and compositionally well-defined Ni_3Ga, the annealed Ni_3Ga exhibited catalytic performance that was considerably different from monometallic Ni and Ni-rich Ni_3Ga. Selectivity approached a nearly ideal H_2/CO_2 product with quite low CH_4 and CO selectivities. The catalyst also exhibited TOF comparable to other leading catalysts and very good stability over 35 h of tests (see Figure 3b). The new surface chemistry of the Ni_3Ga catalyst clearly allowed for sufficient C−H activation and $C/CH_x/CO$ oxidation, but also inhibited unselective rehydrogenation and CH_4 production. After the reaction, characterization showed that the Ni_3Ga bulk phase purity was preserved and some Ni was drawn to the particle surfaces ($[Ni]_{surf,t=0}$ = 77% to $[Ni]_{surf,t=16h}$ = 87%; see Figure 3d). The particle size change was also minor after 16 h (see Figure 3d). The initial conversion was 88% and reduced via the first-order deactivation in the first 6 h and then transitioned to the zeroth-order deactivation (shown in Figure S2). The degree of overall deactivation was significantly less than those of Ni and Ni-rich Ni_3Ga. In the latter case, the larger particles of the annealed catalyst may contribute to their improved stability. During the short deactivation period, the production of CH_4 diminished rapidly with a concomitant increase in the H_2 production, suggesting that Ni-rich surface sites were being either removed or poisoned by Ni carbonyl or coke/carbide formation. Postreaction analysis of the catalyst for coke/carbide formation showed significantly reduced amounts of carbon deposition/incorporation. From oxidative TGA, coke was estimated at only 0.55 wt % of the total weight of the postreaction annealed Ni_3Ga catalyst after 35 h of TOS (Figure S10). This was lower than the as-reduced Ni_3Ga (∼1.3 wt %) and markedly lower than the monometallic Ni catalyst (∼12 wt %).

III.B. Performance of Higher-Energy Ni + Ga IMC Phase Catalysts. Higher-energy Ni + Ga IMC phases were studied to understand the effect of Ni:Ga ratio on the catalytic surface chemistry and overall IMC stability under reaction

https://dx.doi.org/10.1021/acscatal.0c01261
ACS Catal. 2020, 10, 8968−8980

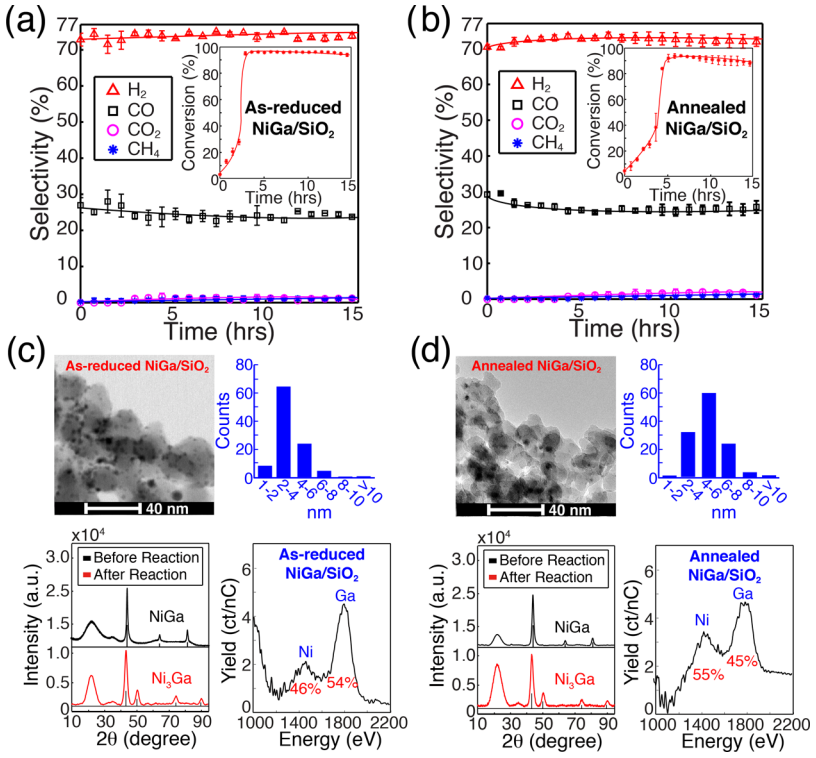

Figure 4. Catalytic performance of (a) as-reduced $NiGa/SiO_2$ and (b) annealed $NiGa/SiO_2$ at 600 °C with S/C = 3, (c) and (d) TEM, long-acquisition-time XRD, and HS-LEIS characterization for fresh as-reduced and annealed $NiGa/SiO_2$, respectively. Both the as-reduced $NiGa/SiO_2$ and annealed $NiGa/SiO_2$ catalyst loadings were 150 mg.

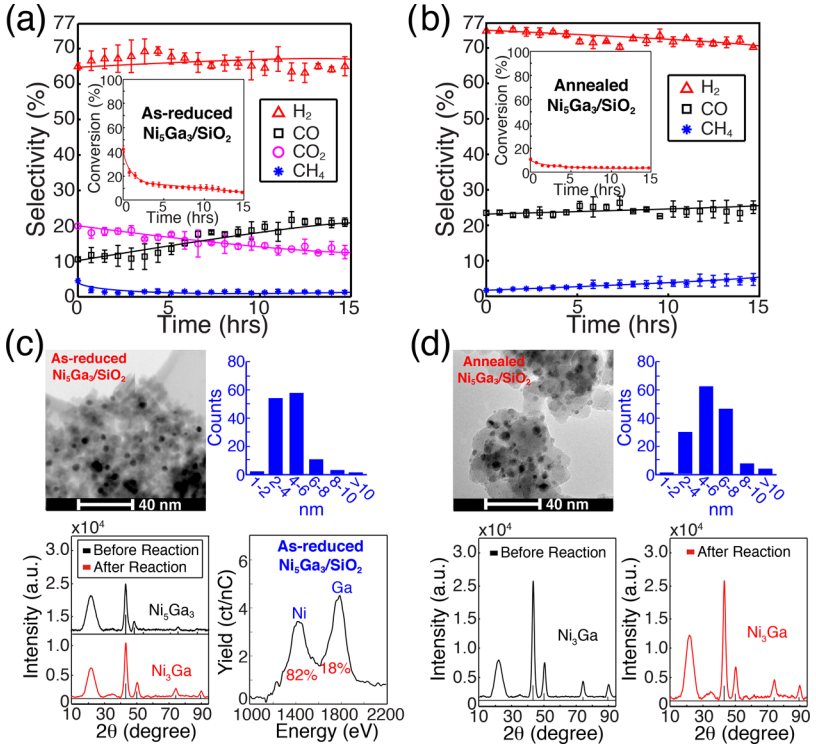

Figure 5. Catalytic performance of (a) as-reduced Ni_5Ga_3/SiO_2 and (b) annealed Ni_5Ga_3/SiO_2 at 400 °C with S/C = 3, (c) and (d) TEM, particle size distribution, long-acquisition-time pXRD, and HS-LEIS characterization of the as-reduced and annealed Ni_5Ga_3/SiO_2, respectively. Both the as-reduced Ni_5Ga_3/SiO_2 and annealed Ni_5Ga_3/SiO_2 catalyst loadings were 800 mg.

conditions. The higher-energy phase NiGa could be synthesized with phase-pure bulk and bulk-like termination in the as-reduced (46% Ni and 54% Ga) and annealed (55% Ni and 45% Ga) cases. Conversely, Ni_5Ga_3, an even higher-energy phase, could be synthesized with phase-pure bulk in the as-reduced form but exhibited a surface composition that was

https://dx.doi.org/10.1021/acscatal.0c01261
ACS Catal. 2020, 10, 8968−8980

Ni_3Ga-like (82% Ni and 18% Ga). Upon annealing, Ni_5Ga_3 bulk relaxed to Ni_3Ga with an unknown surface composition. In either the as-reduced or annealed forms, NiGa and Ni_5Ga_3 exhibited lower propane conversion compared to Ni_3Ga, indicating a reduced surface reactivity toward the activation of propane. NiGa was inactive at 400 °C necessitating higher temperatures (600 °C) (see Figure S7), whereas Ni_5Ga_3 exhibited a moderate activity at 400 °C. In all cases, the bulk of the four catalysts relaxed to Ni_3Ga under reaction conditions. Interestingly, this change dramatically increased the propane conversion in the case of NiGa, but not in the case of Ni_5Ga_3. The NiGa catalysts exhibited similar and nearly ideal selectivity toward H_2 and CO productions, with no clear effect of particle size or bulk phase change (see Figure 4). In addition, zeroth-order deactivation for both the as-reduced and annealed NiGa catalysts was observed after 3−5 h when conversion increased to ∼95 and ∼90%, respectively (see Figure S3). Characterization of coke deposition indicated that little to no carbon was deposited after 15 h of TOS (Figure S10). Conversely, the as-reduced and annealed Ni_5Ga_3 showed marked selectivity differences (see Figure 5). The selectivity of the as-reduced Ni_5Ga_3 at $t = 0$ was 20% CO_2 and 11% CO, but shifted to 12% CO_2 and 21% CO over the 15 h of run. The annealed Ni_5Ga_3 produced nearly ideal selectivity toward H_2 and CO. In all cases, the production of CH_4 was minor, illustrating the control of rehydrogenation kinetics over the IMCs. The bulk phase relaxation to Ni_3Ga of both NiGa and Ni_5Ga_3 likely resulted in a Ga-rich particle surface composition that clearly limited CO oxidation for CO_2 formation. Ni_5Ga_3 was also investigated at 600 °C and showed high conversion but similar product selectivity as runs at 400 °C. Beyond the changes in the catalytic surface chemistry, these results also serve to illustrate the effect of the relative IMC phase stability and reaction conditions on the material stability of IMC catalysts.

Returning to the Ni_3Ga catalyst, water gas shift reactions were performed with a H_2O/CO feed composition that may replicate the environment produced under reforming conditions (H_2O/CO/Ar = 8.1/0.45/95). These investigations were aimed at understanding (i) the connection between the presence of propane fragments and CO_2 selectivity and (ii) the hydrogenation of CO or CO_2 by *in situ* H_2. Results show that both the as-reduced and annealed Ni_3Ga achieve 100% conversion of CO with a nearly ideal 1:1 H_2/CO_2 product selectivity at 400 °C, which suggested that the CO_2 selectivity in the reforming reaction condition was likely due to more efficient CO oxidation and not the oxidation of CH_x fragments that have not been completely stripped of hydrogen (see Figure S11). Additionally, the complete absence of CH_4 as a product under WGS conditions illustrates that limited hydrogenated kinetics over Ni + Ga IMCs is a general feature and not specific to the wet-reforming condition. This view is in line with our previous studies focused on controlling hydrogenation.[20,21,33] This trend is further underscored by the fact that CH_4 is often a major unselective product in WGS when catalyzed by platinum group metals.[52−54] It is interesting to note that despite the as-reduced Ni_3Ga presenting a Ni-dominated surface composition, its performance in the water gas shift was very similar to the Ni_3Ga-terminated annealed Ni_3Ga catalyst.

Because the annealed Ni_3Ga exhibited such a promising catalytic performance, the catalyst was further investigated at lower steam-to-carbon ratios to determine the role of reaction conditions. Surprisingly, the annealed Ni_3Ga exhibited very similar activity and product selectivity with reduced steam-to-carbon ratios of 2:1 and even 1:1, which was not possible over many other common reforming catalysts (see Figure S12). This performance is quite impressive and economically beneficial due to the cost associated with H_2O vaporization. Over many other catalysts, a reduced supply of O/OH groups at lower H_2O chemical potentials often results in increased coke formation, reduced H_2 formation, and increased CO production.[23,55−57] Only slight changes in product distributions as a function of the steam-to-carbon ratio further suggested that appropriately balanced surface reactivity toward C, O, and H over the annealed Ni_3Ga has been achieved.

IV. DISCUSSION

In the efforts to design improved hydrocarbon wet-reforming catalysts, many have focused upon the observation that the initial C−H bond cleavage is rate-determining at steady state and the need for more reactive sites that do not promote coke formation.[46,47,58−62] The exact degree of reactivity needed is not yet clear, but one may predict that it needs to be less than the high-energy sites presented over a fresh Ni catalyst and more reactive than the Ni sites remaining after a steady-state activity is achieved and C−H activation is rate-determining. Moreover, the elevated reactivity of higher-energy Ni sites may not always lead to coke deposition if the C/CH_x fragments are effectively stripped off the surface by rapid oxidation events and reaction sites are homogeneous with respect to providing both C/CH_x and oxidizer species in spatial proximity.

In this view, our results suggest that the Ni + Ga IMCs present a moderate range of surface reactivity toward initial C−H activation of propane that is lower than the over-reactive sites on a fresh Ni catalyst but still aggressive enough to produce TOF compatible to established catalysts at similar temperatures (see Table S2 and refs 17, 22, 63). From propane conversion trends, the surface reactivity toward C−H activation is predicted to track as Ni_3Ga > Ni_5Ga_3 > NiGa, which correlated well with the initial surface compositions of Ni + Ga IMCs. The surface chemistry of the as-reduced Ni_5Ga_3 with an initial surface composition of Ni_3Ga appears to be less reactive than that of the bulk-like terminated Ni_3Ga, suggesting the presence of some amount of extra Ga at the catalyst surface that blocks over-reactive sites. However, this difference in surface composition could not be captured using HS-LEIS measurements.

Results from basic computational surface science studies of initial propane dissociation over model crystal surfaces of the three well-defined Ni + Ga IMC catalysts corroborate predicted surface reactivity (Figure 6). A similar trend was also observed in our prior studies of ethane and propane direct dehydrogenations for olefin production over Ni_3Ga with bulk-like and modified surface Ni:Ga ratios.[20,21] In these studies, surface reactivity toward carbon was attenuated systematically as the Ga surface concentration increased from 25 to 50% and tracked well with high selectivity in the olefin product. We have also shown that Ni IMC surface reactivity toward carbon tracks as a function of the p-element size and orbital overlap in Ni+B-group IMCs with 1:1 element ratios in the semi-hydrogenation of acetylene to ethylene.[33] Similar trends also are apparent when utilizing IMC catalysts produced using larger late TMs (Pt + Sn, Pd + Sn, Pd + In, and Pd + Ga) in olefin production and functionalization reactions.[64−74] Therefore, it is clear that systematic changes in the surface chemistry

https://dx.doi.org/10.1021/acscatal.0c01261
ACS Catal. 2020, 10, 8968−8980

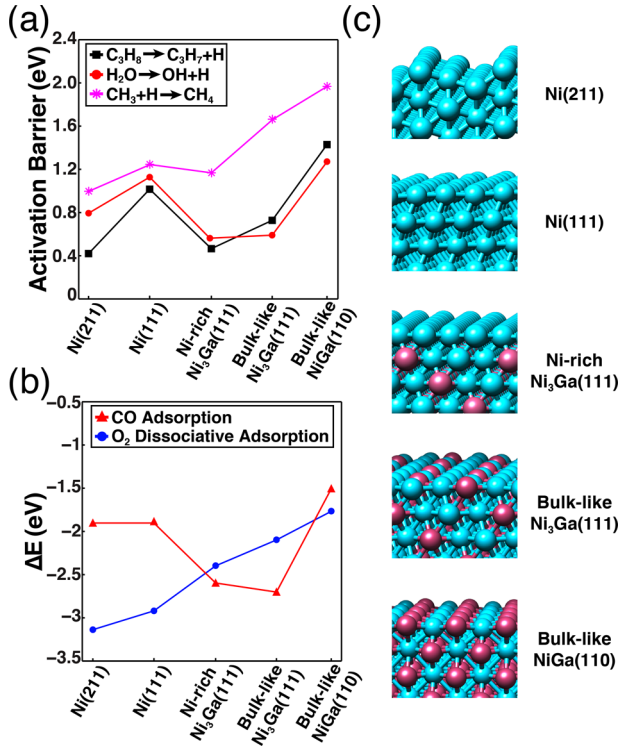

Figure 6. Probe DFT calculations for the investigation of surface reactivity toward C, H, and O over Ni(211), Ni(111), Ni-rich surface $Ni_3Ga(111)$, bulk-like terminated $Ni_3Ga(111)$, and bulk-like terminated NiGa(110). (a) Activation barriers for the first dehydrogenation of propane, H_2O dissociation, and CH_3 hydrogenation to CH_4. (b) Molecular CO and O_2 dissociative adsorption energies. The elements in the slab model systems are color-coded: Ni (light blue) and Ga (magenta).

of late TM IMCs are present and can be rationally selected to investigate fundamental surface reaction mechanisms and tune catalyst performance.

Because non-noble metal IMC catalysts are composed of more reactive elements, insights into surface composition changes driven by reaction conditions are of significant interest. These changes may be driven either by the innate stability of the IMC or by surface-bound reaction intermediates. Focusing on the Ni_3Ga catalysts, the Ni concentration of the as-reduced Ni_3Ga reduced from 92 to 80% Ni and increased from 77 to 87% for the reduced and annealed Ni_3Ga. Because the as-reduced Ni_3Ga with a Ni-rich surface composition can be transformed into bulk-like terminated Ni_3Ga via extended annealing under Ar, we predict that these changes are not driven by innate thermodynamics of the Ni_3Ga phase but by surface-bound intermediates. As mentioned previously, the formation of Ni carbonyl species may remove Ni from the IMC surface, but clearly this effect eventually becomes unfavorable given the slightly Ni-rich surface compositions measured by HS-LEIS for both catalysts after 16 h under reaction conditions. In the case of bulk-like terminated Ni_3Ga, it is unclear exactly which surface-bound reaction intermediate pulls Ni to the surface, but it is suggested that C/CH_x groups or atomic H are responsible. Given that a high chemical potential of H produces a Ni-rich surface in the case of the as-reduced Ni_3Ga and the innate reactivity of Ni toward carbon, both C/CH_x and H may play considerable roles in driving IMC surface composition changes. Interestingly, the relatively high reactivity of Ga toward O/OH appears to not pull Ga to the surface. Moreover, results suggest that the initial starting surface composition also plays a role in the steady-state IMC surface composition under reaction conditions. It is understood that the stability of the elements in the catalyst surface and element-specific reactivity toward intermediates dictate how alloy and solid compound surface compositions change as a function of reaction conditions,[26,75−77] but an overarching fundamental framework to understand and predict the phenomenon still needs to be developed.

The catalytic activity and selectivity trends of the NiGa and Ni_5Ga_3 catalysts that relax to a bulk crystal phase of Ni_3Ga with unknown surface compositions are much more difficult to predict, yet in both cases, it is clear that the new surface composition limits CO oxidation almost entirely. These catalysts are being investigated more thoroughly for a future report, but it is predicted that extra Ga is present at the particle surface given the bulk-like terminated NiGa exhibited the same preference for CO production before bulk phase relaxation to Ni_3Ga. However, this prediction does not agree with the trends observed in surface chemistry toward propane activation as a function of the surface Ga concentration over the well-defined catalysts. Clearly, a special set of surface reaction sites were produced under reaction conditions as NiGa relaxed to Ni_3Ga, yet were absent on the surface of Ni_5Ga_3 after relaxation to Ni_3Ga. Further studies are needed to understand this phenomenon, as it appears to be a clear core−shell-type surface chemistry effect. Moreover, IMC catalyst stability under reaction conditions also needs to be better understood, yet results suggest that both bulk IMC phase stability and the chemical potential of surface-bound intermediates or products play a role in driving bulk phase and surface composition changes for higher-energy IMC phases.

The tunability of CO vs CO_2 selectivity is clearly achievable by modifying the composition of the Ni + Ga IMC catalysts in the bulk and at the particle surface. CO vs CO_2 selectivity may be controlled by either the rate of the second oxygen addition to CO or an OCH_x intermediate, depending on the active mechanism, or the rate of supply or chemical identity of the oxidizer, e.g., O vs OH from H_2O dissociation. In the former case, the balance of carbonaceous intermediate and oxidizer species stability on the catalyst surface would dictate the rate of oxidation.[5,22,23,78] In the latter, the rate of oxidizer supply would be selectivity-controlling.[1,55−57,79,80] As a basis of comparison, Ni is known to drive rapid H_2O dissociation and CH_x/CO oxidation, as determined by many KIE and rate-order studies.[46,47,58−61] This dynamic along with relatively moderate CO adsorption preferentially promotes high CO_2 selectivity.

Some fundamental insight into what controls the CO vs CO_2 selectivity over the Ni + Ga IMC catalysts may be derived from quantum chemical calculations of dissociative adsorption of H_2O and O_2 and molecular adsorption of CO. Comparing Ni(211) to Ni_3Ga indicates that the rate of H_2O dissociation may be similar given similarly low activation barriers. On the other hand, NiGa presents lower surface reactivity in general, a larger barrier for H_2O dissociation ($E_{a,NiGa}$ = 1.3 eV), and slower oxidizer supply kinetics. The kinetics for the CO oxidation step can be roughly predicted by the surface reactivity toward O and CO. Interestingly, both CO and O are less strongly bound over NiGa in comparison to Ni and Ni_3Ga, suggesting more rapid oxidation. Therefore, it is

https://dx.doi.org/10.1021/acscatal.0c01261
ACS Catal. 2020, 10, 8968−8980

suggested that the slow oxidizer supply in competition with a more facile molecular CO desorption contributes to the preferential production of CO over NiGa and the core−shell catalysts produced after NiGa and Ni_5Ga_3 relax to a Ni_3Ga in the bulk. However, a full kinetic network study is needed to fully understand these selectivity trends and will be published in a follow-up report. Nonetheless, others have observed similar selectivity shifts over other alloy and metallic compounds, but the origin of these changes may be mechanistically diverse depending on the balance of constituent rates in the kinetic network.[23,55,57,81]

Limiting the unselective rehydrogenation of propane breakdown intermediates that lead to a lighter hydrocarbon production is critical to enhancing the overall reforming efficiency. Due to the likelihood of an intermediate-laden surface when operating at appreciable conversions, rehydrogenation selectivity will be a strong function of the kinetics of hydrogen transfer from the surface to carbonaceous intermediates and, potentially, a function of hydrocarbon breakdown and oxidation kinetics through kinetic coupling. The known ability of Ni to drive hydrogenation reactions at low temperatures correlates well with the elevated production of CH_4 over the Ni catalyst (refs 4, 17, 23) and the as-prepared as-reduced Ni_3Ga catalyst that exhibited a Ni-dominated surface composition. The diminishing CH_4 production over the latter catalyst as TOS increased the tracks well, with the IMC surface composition shifting to more bulk-like. The trend of limited unselective dehydrogenation is also evident over the well-defined annealed Ni_3Ga and NiGa cases and the less well-defined Ni_5Ga_3 case that was Ni_3Ga-terminated at t = 0 TOS. It is also noted that inhibited hydrogenation was also observed in the WGS reaction tests over the annealed Ni_3Ga catalyst where no CH_4 was produced. In comparison, WGS tests performed over noble metals or monometallic catalysts often result in hydrogen loss to CH_4 production.[52−54]

It is clear that hydrogenation kinetics is inherently limited over the Ni + Ga IMCs. This useful surface chemical feature has been connected to more covalent bonding in the IMC that modifies H-surface bonding and hydrogen transfer kinetics. This same phenomenon was encountered in our prior studies of semihydrogenation of acetylene over Ni+B-group IMCs and was found to track well with the degree of covalent-like bonding within the IMC, which tracked with the orbital−orbital overlap between the constituent elements.[33] Most notably, limited hydrogenation kinetics was observed over NiAl and NiGa where orbital overlap was the greatest between Ni and the boron group elements investigated. Our studies of Ni_3Ga with the modified surface Ga concentration in the direct dehydrogenation of propane and ethane for olefin production also illustrated the limited hydrogenation kinetics over Ni + Ga IMCs as a function of the surface composition.[20,21] Interestingly, the same control of hydrogenation kinetics was observed over solid TM compounds produced using nonmetal elements, which suggests a quite general trend in surface chemistry that connects all TM solid compounds formed through reaction with p-block elements.[34] Several other studies have also noted this interesting electronic effect in more focused studies.[71,72,82] Also interesting is that the limited hydrogenation kinetics appears to not detrimentally affect H_2 evolution, which may suggest that the electronic effect is species-specific or marked H-surface coverage effects are present that promote H_2 evolution because unselective dehydrogenation is kinetically inhibited.

V. CONCLUSIONS

Systematic control of surface and catalytic chemistry of Ni + Ga IMC catalysts was possible through the manipulation of bulk and surface compositions. Compared with pure Ni catalyst, Ni + Ga IMC catalysts, with new electronic structures, exhibited newly accessible surface reactivity toward C, H, and O that appeared to be appropriately balanced for the wet reforming of C_{2+}-saturated hydrocarbons. Nearly ideal product selectivity toward either H_2/CO or H_2/CO_2 could be achieved under the same reaction conditions depending on catalyst formulation. Dramatically reduced coke deposition and enhanced catalyst stability were also achieved. At the fundamental mechanistic level, limited coke formation with retained overall activity was achieved by tuning the surface reactivity toward C−H activation to be less than that of Ni(211) but greater than that of Ni(111). CO vs CO_2 selectivity was found to be controlled by a competition between molecular CO desorption and CO oxidation and water dissociation kinetics. The beneficial limiting of unselective rehydrogenation kinetics was connected to the more covalent bonding within the IMC, new H-surface bonding, and was shown to be a general trend over TM solid compounds composed of TMs and p-block elements.

■ ASSOCIATED CONTENT

Supporting Information

The Supporting Information is available free of charge at https://pubs.acs.org/doi/10.1021/acscatal.0c01261.

Experimental method includes catalyst characterization and the calculation method; deactivation order analysis of as-reduced Ni_3Ga/SiO_2, a is relative activity, (a) 2nd order; (b) 1st order; (c) zeroth order (Figure S1); deactivation order analysis of annealed Ni_3Ga/SiO_2. a is relative activity, (a) 2nd order; (b) 1st order; (c) zeroth order (Figure S2); deactivation order analysis of (a) as-reduced $NiGa/SiO_2$ and (b) annealed $NiGa/SiO_2$, a is relative activity (Figure S3); ICP-AES quantification of the composition of SiO_2 supported Ni + Ga catalysts; the number in parenthesis is the actual loading (Table S1); TOF rates of propane for the catalysts under investigation and a summary of the catalytic data of the published work for comparison (Table S2) (PDF)

■ AUTHOR INFORMATION

Corresponding Author

Siris Laursen − *Department of Chemical and Biomolecular Engineering, University of Tennessee, Knoxville, Tennessee 37996, United States;* orcid.org/0000-0002-5769-7393; Email: slaursen@utk.edu

Authors

Yuanjun Song − *Department of Chemical and Biomolecular Engineering, University of Tennessee, Knoxville, Tennessee 37996, United States*

Yang He − *Department of Chemical and Biomolecular Engineering, University of Tennessee, Knoxville, Tennessee 37996, United States*

Complete contact information is available at: https://pubs.acs.org/10.1021/acscatal.0c01261

Notes

The authors declare no competing financial interest.

https://dx.doi.org/10.1021/acscatal.0c01261
ACS Catal. 2020, 10, 8968−8980

■ ACKNOWLEDGMENTS

This research was supported by the National Science Foundation (NSF) CAREER award (Grant CBET-1752063) and the American Chemical Society Petroleum Research Fund (Grant PRF# 57589-ND5). This work used the Extreme Science and Engineering Discovery Environment (XSEDE), which is supported by the National Science Foundation (Project TG-CTS140009).[83] XRD analyses were conducted at the Center for Nanophase Materials Sciences (CNMS project number CNMS2018-374) at Oak Ridge National Lab (ORNL).

■ REFERENCES

(1) Krcha, M. D.; Janik, M. J. Catalytic Propane Reforming Mechanism over Zr-doped CeO_2(111). *Catal. Sci. Technol.* **2014**, *4*, 3278.
(2) Xie, C.; Chen, Y.; Engelhard, M. H.; Song, C. Comparative Study on the Sulfur Tolerance and Carbon Resistance of Supported Noble Metal Catalysts in Steam Reforming of Liquid Hydrocarbon Fuel. *ACS Catal.* **2012**, *2*, 1127.
(3) Haghofer, A.; Föttinger, K.; Girgsdies, F.; Teschner, D.; Knop-Gericke, A.; Schlögl, R.; Rupprechter, G. In situ Study of the Formation and Stability of Supported Pd_2Ga Methanol Steam Reforming Catalysts. *J. Catal.* **2012**, *286*, 13.
(4) Malaibari, Z. O.; Croiset, E.; Amin, A.; Epling, W. Effect of Interactions between Ni and Mo on Catalytic Properties of a Bimetallic Ni-Mo/Al_2O_3 Propane Reforming Catalyst. *Appl. Catal., A* **2015**, *490*, 80.
(5) Ota, A.; Kunkes, E. L.; Kasatkin, I.; Groppo, E.; Ferri, D.; Poceiro, B.; Navarro Yerga, R. M.; Behrens, M. Comparative Study of Hydrotalcite-derived Supported Pd_2Ga and PdZn Intermetallic Nanoparticles as Methanol Synthesis and Methanol Steam Reforming Catalysts. *J.. Catal.* **2012**, 27.
(6) Rameshan, C.; Lorenz, H.; Mayr, L.; Penner, S.; Zemlyanov, D.; Arrigo, R.; Haevecker, M.; Blume, R.; Knop-Gericke, A.; Schlögl, R.; Bernhard, K. CO_2-selective Methanol Steam Reforming on In-doped Pd Studied by in situ X-ray Photoelectron Spectroscopy. *J. Catal.* **2012**, *295*, 186.
(7) Guo, J.; Xie, C.; Lee, K.; Guo, N.; Miller, J. T.; Janik, M. J.; Song, C. Improving the Carbon Resistance of Ni-Based Steam Reforming Catalyst by Alloying with Rh: A Computational Study Coupled with Reforming Experiments and EXAFS Characterization. *ACS Catal.* **2011**, *1*, 574.
(8) Fei, J.; Hou, Z.; Zheng, X.; Yashima, T. Doped Ni Catalysts for Methane Reforming with CO_2. *Catal. Lett.* **2004**, *98*, 241.
(9) Chin, Y.; King, D.; Roh, H.; Wang, Y.; Heald, S. Structure and Reactivity Investigations on Supported Bimetallic AuNi Catalysts Used for Hydrocarbon Steam Reforming. *J. Catal.* **2006**, *244*, 153.
(10) Besenbacher, F. Design of a Surface Alloy Catalyst for Steam Reforming. *Science* **1998**, 1913.
(11) Wu, H.; La Parola, V.; Pantaleo, G.; Puleo, F.; Venezia, A.; Liotta, L. Ni-Based Catalysts for Low Temperature Methane Steam Reforming: Recent Results on Ni-Au and Comparison with Other Bi-Metallic Systems. *Catalysts* **2013**, *3*, 563.
(12) Bengaard, H.; Nørskov, J.; Sehested, J.; Clausen, B.; Nielsen, L.; Molenbroek, A.; Rostrup-Nielsen, J. Steam Reforming and Graphite Formation on Ni Catalysts. *J. Catal.* **2002**, *209*, 365.
(13) Parizotto, N.; Rocha, K.; Damyanova, S.; Passos, F.; Zanchet, D.; Marques, C.; Bueno, J. Alumina-supported Ni Catalysts Modified with Silver for the Steam Reforming of Methane: Effect of Ag on the Control of Coke Formation. *Appl. Catal., A* **2007**, *330*, 12.
(14) Palma, S.; Bobadilla, L.; Corrales, A.; Ivanova, S.; Romero-Sarria, F.; Centeno, M.; Odriozola, J. Effect of Gold on a $NiLaO_3$ Perovskite Catalyst for Methane Steam Reforming. *Appl. Catal., B* **2014**, *144*, 846.
(15) Tomishige, K.; Li, D.; Tamura, M.; Nakagawa, Y. Nickel-Iron Alloy Catalysts for Reforming of Hydrocarbons: Preparation, Structure, and Catalytic Properties. *Catal. Sci. Technol.* **2017**, *7*, 3952.
(16) Koike, M.; Li, D.; Nakagawa, Y.; Tomishige, K. A Highly Active and Coke-Resistant Steam Reforming Catalyst Comprising Uniform Nickel-Iron Alloy Nanoparticles. *ChemSusChem* **2012**, *5*, 2312.
(17) Li, Y.; Wang, X.; Xie, C.; Song, C. Influence of Ceria and Nickel Addition to Alumina-supported Rh Catalyst for Propane Steam Reforming at Low Temperatures. *Appl. Catal., A* **2009**, *357*, 213.
(18) Huber, G. W. Raney Ni-Sn Catalyst for H_2 Production from Biomass-Derived Hydrocarbons. *Science* **2003**, *300*, 2075.
(19) Studt, F.; Sharafutdinov, I.; Abild-Pedersen, F.; Elkjær, C. F.; Hummelshoj, J. S.; Dahl, S.; Chorkendorff, I.; Norskov, J. K. Discovery of a Ni-Ga Catalyst for Carbon Dioxide Reduction to Methanol. *Nat. Chem.* **2014**, *6*, 320.
(20) He, Y.; Song, Y.; Cullen, D. A.; Laursen, S. Selective and Stable Non-Noble-Metal Intermetallic Compound Catalyst for the Direct Dehydrogenation of Propane to Propylene. *J. Am. Chem. Soc.* **2018**, *140*, 14010.
(21) He, Y.; Song, Y.; Laursen, S. The Origin of the Special Surface and Catalytic Chemistry of Ga-Rich Ni_3Ga in the Direct Dehydrogenation of Ethane. *ACS Catal.* **2019**, *9*, 10464.
(22) Natesakhawat, S.; Oktar, O.; Ozkan, U. S. Effect of Lanthanide Promotion on Catalytic Performance of Sol-Gel Ni/Al_2O_3 Catalysts in Steam Reforming of Propane. *J. Mol. Catal. A: Chem.* **2005**, *241*, 133.
(23) Natesakhawat, S.; Watson, R.; Wang, X.; Ozkan, U. Deactivation Characteristics of Lanthanide-Promoted Sol-Gel Ni/Al_2O_3 Catalysts in Propane Steam Reforming. *J. Catal..* **2005**, *234*, 496.
(24) Saadi, S.; Hinnemann, B.; Helveg, S.; Appel, C.; Abild-Pedersen, F.; Norskov, J. First-principles Investigations of the Ni_3Sn Alloy at Steam Reforming Conditions. *Surf. Sci.* **2009**, *603*, 762.
(25) Neumann, M.; Teschner, D.; Knop-Gericke, A.; Reschetilowski, W.; Armbrüster, M. Controlled Synthesis and Catalytic Properties of Supported In-Pd Intermetallic Compounds. *J. Catal.* **2016**, *340*, 49.
(26) Friedrich, M.; Teschner, D.; Knop-Gericke, A.; Armbrüster, M. Influence of Bulk Composition of the Intermetallic Compound ZnPd on Surface Composition and Methanol Steam Reforming Properties. *J. Catal.* **2012**, *285*, 41.
(27) Wang, L.; Hisada, Y.; Koike, M.; Li, D.; Watanabe, H.; Nakagawa, Y.; Tomishige, K. Catalyst Property of Co-Fe Alloy Particles in the Steam Reforming of Biomass Tar and Toluene. *Appl. Catal., B* **2012**, *121−122*, 95.
(28) Boudart, M. Thermodynamic and Kinetic Coupling of Chain and Catalytic Reactions. *J. Phys. Chem. A.* **1983**, *87*, 2786.
(29) Boudart, M.; Djéga-Mariadassou, G. Kinetic Coupling in and between Catalytic Cycles. *Catal. Lett.* **1994**, *29*, 7.
(30) Djéga-Mariadassou, G.; Boudart, M. Classical Kinetics of Catalytic Reactions. *J. Catal.* **2003**, *216*, 89.
(31) Hu, X.; Lu, G. Inhibition of Methane Formation in Steam Reforming Reactions through Modification of Ni Catalyst and the Reactants. *Green Chem.* **2009**, *11*, 724.
(32) Velu, S.; Suzuki, K.; Osaki, T. A Comparative Study of Reactions of Methanol over Catalysts Derived from NiAl- and CoAl-layered Double Hydroxides and their Sn-containing Analogues. *Catal. Lett.* **2000**, *69*, 43.
(33) Song, Y.; Laursen, S. Control of Surface Reactivity towards Unsaturated C-C Bonds and H over Ni-based Intermetallic Compounds in Semi-hydrogenation of Acetylene. *J. Catal.* **2019**, *372*, 151.
(34) He, Y.; Laursen, S. Trends in the Surface and Catalytic Chemistry of Transition-Metal Ceramics in the Deoxygenation of a Woody Biomass Pyrolysis Model Compound. *ACS Catal.* **2017**, *7*, 3169.
(35) Li, L.; Zhang, B.; Kunkes, E.; Föttinger, K.; Armbrüster, M.; Su, D. S.; Wei, W.; Schlögl, R.; Behrens, M. Ga-Pd/Ga_2O_3 Catalysts: The Role of Gallia Polymorphs, Intermetallic Compounds, and Pretreatment Conditions on Selectivity and Stability in Different Reactions. *ChemCatChem* **2012**, *4*, 1764.

https://dx.doi.org/10.1021/acscatal.0c01261
ACS Catal. 2020, 10, 8968−8980

(36) Friedrich, M.; Penner, S.; Heggen, M.; Armbrüster, M. High CO_2 Selectivity in Methanol Steam Reforming through ZnPd/ZnO Teamwork. *Angew. Chem., Int. Ed.* **2013**, *52*, 4389.
(37) Furukawa, S.; Komatsu, T. Intermetallic Compounds: Promising Inorganic Materials for Well-Structured and Electronically Modified Reaction Environments for Efficient Catalysis. *ACS Catal.* **2016**, *7*, 735.
(38) Fan, Z.; Zhang, H. Crystal Phase-Controlled Synthesis, Properties and Applications of Noble Metal Nanomaterials. *Chem. Soc. Rev.* **2016**, *45*, 63.
(39) Datye, A. K.; Xu, Q.; Kharas, K. C.; McCarty, J. M. Particle Size Distributions in Heterogeneous Catalysts: What do They Tell Us about the Sintering Mechanism. *Catal. Today* **2006**, *111*, 59.
(40) Behafarid, F.; Pandey, S.; Diaz, R. E.; Stach, E. A.; Cuenya, B. R. An in situ Transmission Electron Microscopy Study of Sintering and Redispersion Phenomena over Size-Selected Metal Nanoparticles: Environmental Effects. *Phys. Chem. Chem. Phys.* **2014**, *16*, 18176.
(41) Campbell, C. T. The Energetics of Supported Metal Nanoparticles: Relationships to Sintering Rates and Catalytic Activity. *Acc. Chem. Res.* **2013**, *46*, 1712.
(42) Rakib, M. A.; Grace, J. R.; Lim, C. J.; Elnashaie, S. S.; Ghiasi, B. Steam Reforming of Propane in a Fluidized Bed Membrane Reactor for Hydrogen Production. *Int. J. Hydrogen Energy* **2010**, *35*, 6276.
(43) Matsuka, M.; Shigedomi, K.; Ishihara, T. Comparative Study of Propane Steam Reforming in Vanadium Based Catalytic Membrane Reactor with Nickel-Based Catalysts. *Int. J. Hydrogen Energy* **2014**, *39*, 14792.
(44) Che, F.; Hensley, A. J.; Ha, S.; McEwen, J. S. Decomposition of Methyl Species on a Ni(211) Surface: Investigations of the Electric Field Influence. *Catal. Sci. Technol.* **2014**, *4*, 4020.
(45) Rostrup-Nielsen, J.; Nørskov, J. K. Step Sites in Syngas Catalysis. *Top. Catal.* **2006**, *40*, 45.
(46) Wei, J.; Iglesia, E. Isotopic and Kinetic Assessment of the Mechanism of Methane Reforming and Decomposition Reactions on Supported Iridium Catalysts. *Phys.. Chem. Chem. Phys.* **2004**, *6*, 3754.
(47) Wei, J.; Iglesia, E. Reaction Pathways and Site Requirements for the Activation and Chemical Conversion of Methane on Ru-Based Catalysts. *J. Phys. Chem. B* **2004**, *108*, 7253.
(48) Wang, Z.; Cao, X.; Zhu, J.; Hu, P. Activity and Coke Formation of Nickel and Nickel Carbide in Dry Reforming: A Deactivation Scheme from Density Functional Theory. *J. Catal.* **2014**, *311*, 469.
(49) Catapan, R. C.; Oliveira, A. A. M.; Chen, Y.; Vlachos, D. G. DFT Study of the Water-Gas Shift Reaction and Coke Formation on Ni(111) and Ni(211) Surfaces. *J. Phys. Chem. C* **2012**, *116*, 20281.
(50) Zhou, M.; Liu, B. First-Principles Investigation of Adsorbate-Adsorbate Interactions on Ni(111), Ni(211), and Ni(100) Surfaces. *Ind. Eng. Chem. Res.* **2017**, *56*, 5813.
(51) Blaylock, D. W.; Zhu, Y. A.; Green, W. H. Computational Investigation of the Thermochemistry and Kinetics of Steam Methane Reforming Over a Multi-Faceted Nickel Catalyst. *Top. Catal.* **2011**, *54*, 828.
(52) Utaka, T.; Okanishi, T.; Takeguchi, T.; Kikuchi, R.; Eguchi, K. Water Gas Shift Reaction of Reformed Fuel over Supported Ru Catalysts. *Appl. Catal., A* **2003**, *245*, 343.
(53) Saw, E.; Oemar, U.; Tan, X.; Du, Y.; Borgna, A.; Hidajat, K.; Kawi, S. Bimetallic Ni-Cu Catalyst Supported on CeO_2 for High-Temperature Water-Gas Shift Reaction: Methane Suppression via Enhanced CO Adsorption. *J. Catal.* **2014**, *314*, 32.
(54) Watanabe, K.; Miyao, T.; Higashiyama, K.; Yamashita, H.; Watanabe, M. Preparation of a Mesoporous Ceria-Zirconia Supported Ni-Fe Catalyst for the High Temperature Water-Gas Shift Reaction. *Catal. Commun.* **2011**, *12*, 976.
(55) Hardiman, K. M.; Ying, T. T.; Adesina, A. A.; Kennedy, E. M.; Dlugogorski, B. Z. Performance of a Co-Ni Catalyst for Propane Reforming under Low Steam-to-Carbon Ratios. *Chem. Eng. J.* **2004**, *102*, 119.
(56) Schädel, B. T.; Duisberg, M.; Deutschmann, O. Steam Reforming of Methane, Ethane, Propane, Butane, and Natural Gas over a Rhodium-based catalyst. *Catal. Today* **2009**, *142*, 42.
(57) Christensen, K.; Chen, D.; Lødeng, R.; Holmen, A. Effect of Supports and Ni Crystal Size on Carbon Formation and Sintering during Steam Methane Reforming. *Appl. Catal., A* **2006**, *314*, 9.
(58) Aparicio, L. Transient Isotopic Studies and Microkinetic Modeling of Methane Reforming over Nickel Catalysts. *J. Catal.* **1997**, *165*, 262.
(59) Kroll, V.; Swaan, H.; Lacombe, S.; Mirodatos, C. Methane Reforming Reaction with Carbon Dioxide over Ni/SiO_2 Catalyst. *J. Catal.* **1996**, *164*, 387.
(60) Otsuka, K.; Kobayashi, S.; Takenaka, S. Hydrogen-Deuterium Exchange Studies on the Decomposition of Methane over Ni/SiO_2. *J. Catal.* **2001**, *200*, 4.
(61) Luo, J.; Yu, Z.; Ng, C.; Au, C. CO_2/CH_4 Reforming over Ni–La_2O_3/5A: An Investigation on Carbon Deposition and Reaction Steps. *J. Catal.* **2000**, *194*, 198.
(62) Rostrupnielsen, J. Activity of Nickel Catalysts for Steam Reforming of Hydrocarbons. *J. Catal.* **1973**, *31*, 173.
(63) Thormann, J.; Maier, L.; Pfeifer, P.; Kunz, U.; Deutschmann, O.; Schubert, K. Steam Reforming of Hexadecane over a Rh/CeO_2 Catalyst in Microchannels: Experimental and Numerical Investigation. *Int. J. Hydrogen Energy* **2009**, *34*, 5108.
(64) Zhao, H.; Koel, B. E. Adsorption and Reaction of 1,3-Butadiene on Pt(111) and Sn/Pt(111) Surface Alloys. *Surf. Sci.* **2004**, *572*, 261.
(65) Cortright, R. D.; Hill, J. M.; Dumesic, J. A. Selective Dehydrogenation of Isobutane over Supported Pt/Sn Catalysts. *Catal. Today* **2000**, *55*, 213.
(66) Breinlich, C.; Haubrich, J.; Becker, C.; Valcarcel, A.; Delbecq, F.; Wandelt, K. Hydrogenation of 1,3-Butadiene on Pd(111) and PdSn/Pd(111) Surface Alloys Under UHV Conditions. *J. Catal.* **2007**, *251*, 123.
(67) Cao, Y.; Sui, Z.; Zhu, Y.; Zhou, X.; Chen, D. Selective Hydrogenation of Acetylene over Pd-In/Al_2O_3 Catalyst: promotional Effect of Indium and Composition-Dependent Performance. *ACS Catal.* **2017**, *7*, 7835.
(68) Armbrüster, M.; Kovnir, K.; Behrens, M.; Teschner, D.; Grin, Y.; Schlögl, R. Pd-Ga Intermetallic Compounds as Highly Selective Semihydrogenation Catalysts. *J. Am. Chem. Soc.* **2010**, *132*, 14745.
(69) Yang, M. L.; Zhu, Y. A.; Zhou, X. G.; Sui, Z. J.; Chen, D. First-Principles Calculations of Propane Dehydrogenation over PtSn Catalysts. *ACS Catal.* **2012**, *2*, 1247.
(70) Snider, J. L.; Streibel, V.; Hubert, M. A.; Choksi, T. S.; Valle, E.; Upham, D. C.; Schumann, J.; Duyar, M. S.; Gallo, A.; Abild-Pedersen, F.; Jaramillo, T. F. Revealing the Synergy between Oxide and Alloy Phases on the Performance of Bimetallic In-Pd Catalysts for CO2 Hydrogenation to Methanol. *ACS Catal.* **2019**, *9*, 3399.
(71) Studt, F.; Abild-Pedersen, F.; Bligaard, T.; Sorensen, R. Z.; Christensen, C. H.; Norskov, J. K. Identification of Non-precious Metal Alloy Catalysts for Selective Hydrogenation of Acetylene. *Science* **2008**, *320*, 1320.
(72) Prinz, J.; Pignedoli, C. A.; Stöckl, Q. S.; Armbrüster, M.; Brune, H.; Gröning, O.; Widmer, R.; Passerone, D. Adsorption of Small Hydrocarbons on the Three-Fold PdGa Surfaces: the Road to Selective Hydrogenation. *J. Am. Chem. Soc.* **2014**, *136*, 11792.
(73) Krajčí, M.; Hafner, J. Intermetallic Compound AlPd As a Selective Hydrogenation Catalyst: a DFT Study. *J. Phys. Chem. C* **2012**, *116*, 6307.
(74) Krajčí, M.; Hafner, J. Complex Intermetallic Compounds as Selective Hydrogenation Catalysts—a Case Study for the (100) Surface of $Al_{13}Co_4$. *J. Catal.* **2011**, *278*, 200.
(75) Zugic, B.; Wang, L.; Heine, C.; Zakharov, D. N.; Lechner, B. A. J.; Stach, E. A.; Biener, J.; Salmeron, M.; Madix, R. J.; Friend, C. M. Dynamic Restructuring Drives Catalytic Activity on Nanoporous Gold-Silver Alloy Catalysts. *Nat. Mater.* **2016**, *16*, 558.
(76) Zafeiratos, S.; Piccinin, S.; Teschner, D. Alloys in Catalysis: Phase Separation and Surface Segregation Phenomena in Response to the Reactive Environment. *Catal. Sci. Technol.* **2012**, *2*, 1787.
(77) Krajčí, M.; Hafner, J. Structure and Chemical Reactivity of the Polar Three-Fold Surfaces of GaPd: A Density-Functional Study. *J. Chem. Phys.* **2013**, *138*, No. 124703.

https://dx.doi.org/10.1021/acscatal.0c01261
ACS Catal. 2020, 10, 8968−8980

(78) Jones, G.; Jakobsen, J.; Shim, S.; Kleis, J.; Andersson, M.; Rossmeisl, J.; Abildpedersen, F.; Bligaard, T.; Helveg, S.; Hinnemann, B. First Principles Calculations and Experimental Insight into Methane Steam Reforming over Transition Metal Catalysts. *J. Catal.* **2008**, *259*, 147.
(79) Kolb, G.; Zapf, R.; Hessel, V.; Löwe, H. Propane Steam Reforming in Micro-channels—results from Catalyst Screening and Optimisation. *Appl. Catal., A* **2004**, *277*, 155.
(80) Krcha, M. D.; Janik, M. J. Catalytic Propane Reforming Mechanism over Mn-Doped CeO_2 (111). *Surf. Sci.* **2015**, *640*, 119.
(81) Li, X.; Li, D.; Tian, H.; Zeng, L.; Zhao, Z. J.; Gong, J. Dry Reforming of Methane over Ni/La_2O_3 Nanorod Catalysts with Stabilized Ni Nanoparticles. *Appl. Catal., B* **2017**, *202*, 683.
(82) Kovnir, K.; Osswald, J.; Armbruster, M.; Teschner, D.; Weinberg, G.; Wild, U.; Knop-Gericke, A.; Ressler, T.; Grin, Y.; Schlogl, R. Etching of the Intermetallic Compounds PdGa and Pd_3Ga_7: an Effective Way to Increase Catalytic Activity? *J. Catal.* **2009**, *264*, 93.
(83) Towns, J.; Cockerill, T.; Dahan, M.; Foster, I.; Gaither, K.; Grimshaw, A.; Hazlewood, V.; Lathrop, S.; Lifka, D.; Peterson, G. D.; Roskies, R.; Ray, S.; Nancy, W. D. XSEDE: Accelerating Scientific Discovery. *Comput. Sci. Eng.* **2014**, *16*, 62.

https://dx.doi.org/10.1021/acscatal.0c01261
ACS Catal. 2020, 10, 8968−8980